AIAA JOURNAL
Vol. 30, No. 3, March 1992

Turbulence Model Effects on Separated Flow About a Prolate Spheroid

Ken Gee* and Russell M. Cummings†
California Polytechnic State University, San Luis Obispo, California 93407
and
Lewis B. Schiff‡
NASA Ames Research Center, Moffett Field, California 94035

The three-dimensional separated flow about a prolate spheroid at high incidence is numerically investigated using the F3D thin-layer Navier-Stokes code. The effect of different turbulence models on the flowfield solution and the characteristics of the predicted flow are analyzed. The models used in this study are the Baldwin-Lomax algebraic model, the Baldwin-Lomax model as modified for crossflow separation by Degani and Schiff, and a modified version of the Johnson-King model with and without the Degani-Schiff crossflow modifications applied. The Johnson-King model is applied to assess the importance of modeling nonequilibrium effects in predicting flow about a slender body at high incidence. The computations are made for steady-state, fully turbulent flow. The results are compared with experimental pressure data and with computational results obtained by Panaras and Steger, using the identical code and grid, but with their own modifications to the Baldwin-Lomax model. In addition, the computed solutions are analyzed using surface flow patterns, helicity density contours, and turbulent eddy-viscosity profiles. The results of this analysis provide insight into the effects of the turbulence models on flow characteristics and demonstrate the effect of the models on the accurate prediction of highly separated and vortical flows about a slender body.

Introduction

CURRENTLY, there is great interest in the handling characteristics of aircraft flying at high angle of attack. Understanding the behavior of the flow about bodies at such flight conditions can lead to increased performance and safety of present and future aircraft designs. There are numerous examples of experimental and computational investigations aimed at determining the effects of three-dimensional separated flow on aircraft and the means of utilizing these effects to the best possible advantage. However, the complexity of the flow makes such analysis a formidable task.

Flight in the high-angle-of-attack region is characterized by massive three-dimensional separated flow about the wing and fuselage. The characteristics of the separated flow about the wing is different from that about the fuselage, and accurate numerical prediction of the flow about both remains a challenge. Generally, prediction of the flowfield features requires the solution of the Navier-Stokes equations. For cases where the Reynolds number indicates that the flow is turbulent, a turbulence model is needed. The accuracy of the computed solutions depends on the numerical algorithm, grid spacing, and turbulence model used. Vatsa et al.[1] focused on the effects of different numerical algorithms and grid spacing on the computed flow about a prolate spheroid. The current work focuses on the effect of different turbulence models on the flow computed about a similar body. By keeping the flow conditions, flow solver, and grid identical in each computation, any differences in the computed solutions are attributable to the turbulence model used.

Although a variety of turbulence models have been proposed, they all invariably suffer from limitations that affect the accuracy and applicability of the models. The more popular models include the Baldwin-Lomax[2] and Johnson-King[3] models. The Baldwin-Lomax model and modifications of this model have been applied to a variety of flow problems, whereas the Johnson-King model, or modified versions thereof, has been applied to airfoil and wing flows, but not to bodies of revolution at high angle of attack.

In this work, three-dimensional separated flow about a prolate spheroid at large incidence is investigated using the F3D thin-layer Navier-Stokes code. The effect of different turbulence models on the flowfield solution and the characteristics of the predicted flow are analyzed. The models used in the present study are the Baldwin-Lomax algebraic model,[2] the Baldwin-Lomax model as modified for crossflow separation by Degani and Schiff,[4] and a form of the Johnson-King model[3] developed by Abid et al.,[5] with and without the Degani-Schiff modifications. The results are compared with experimental data and with computational results obtained by Panaras and Steger,[6] who used the identical code and grid, but with their own modifications to the Baldwin-Lomax model. The accuracy of the computed solutions is assessed qualitatively using surface flow patterns that simulate experimental oil flow pictures and helicity density contours, which show the relative size and strength of the separated vortices. A quantitative measure of accuracy is obtained by comparing surface pressure data to experimental values. An assessment of turbulence model effects on local flowfield parameters is made by examining the turbulent eddy viscosity.

Presented as Paper 90-3106 at the AIAA Applied Aerodynamics Conference, Portland, OR, Aug. 20–22, 1990. Received Oct. 16, 1990; revision received March 23, 1991; accepted for publication March 23, 1991.

*Graduate Research Assistant, Aeronautical Engineering Department; currently at MCAT Institute, Ames Research Center, MS 258-1, Moffett Field, CA 94035. Member AIAA.

†Associate Professor, Aeronautical Engineering Department. Associate Fellow AIAA.

‡Special Assistant for High Alpha Technology, Fluid Dynamics Division, MS 258-1. Associate Fellow AIAA.

Theoretical Background

Governing Equations

The fundamental equations governing fluid flow are based on the laws of mass, momentum, and energy conservation. These conservation laws are used to formulate the Navier-Stokes equations, a set of five coupled, nonlinear partial differential equations that form the basis of viscous flow theory. Typically, simplified forms of the Navier-Stokes equations are used in computational work to save computational time and expense. For a body-oriented coordinate system (ξ, η, ζ) in which one of the coordinates is approximately normal to the body surface (Fig. 1), the thin-layer approximation is used. This approximation retains the viscous terms in the normal, or ζ, direction only. In this work, the application of the thin-layer assumption is justified by noting that the viscous effects are confined to a thin layer near the wall, with the viscous terms in the normal direction being predominant. The remainder of the flowfield is rotational and inviscid. Although viscous effects exist in the vortex sheets that leave the body along the separation lines, such effects are small compared to the convective effects of the inviscid flowfield. Applying the thin-layer approximation, the Navier-Stokes equations are written in terms of nondimensional variables[7] as

$$\partial_\tau \hat{Q} + \partial_\xi \hat{F} + \partial_\eta \hat{G} + \partial_\zeta \hat{H} = Re^{-1} \partial_\zeta \hat{S} \tag{1}$$

In Eq. (1), the viscous terms are collected into the vector $\hat{S}$ and the nondimensional Reynolds number Re is factored from the viscous flux term.

Numerical Algorithm

The numerical scheme employed in this study is the implicit F3D code reported by Steger et al.[8] The algorithm uses flux-vector splitting[9] to upwind difference the convection terms in one coordinate direction (nominally streamwise). This code is utilized because it has been shown to successfully compute the flowfields in a wide variety of aerospace applications, including flow about bodies of revolution, such as ogive cylinders,[10] hemisphere cylinders,[11] and prolate spheroids.[6] Currently, this code is being used to compute the flowfields about the F-18 HARV vehicle[12,13] at flight conditions. Typically, in these computations, the Baldwin-Lomax model,[2] as modified by Degani and Schiff,[4] is used. Thus, results of the current work may enhance the accuracy of future computations. Full details of the algorithm and its development are found in Refs. 8 and 14.

Turbulence Models

To predict turbulent flows by finite-difference solution of the Reynolds-averaged Navier-Stokes equations, it is necessary to make closure assumptions about the apparent turbulent viscous stress and heat-flux quantities. Such assumptions are made by using turbulence models, which use empirically derived equations to determine the turbulent eddy viscosity coefficient. This coefficient, in turn, is used to find the apparent turbulent shear stress values. The models invetigated in this study are the Baldwin-Lomax turbulence model[2] (model A), the Baldwin-Lomax model as modified to account for crossflow separation by Degani and Schiff[4] (model B), and a modified form[5] of the Johnson-King turbulence model[3] (model C). The Degani-Schiff modifications are applied to model C and investigated as a separate model (model D). A list of the turbulence models, and the significant features of each, is given in Table 1.

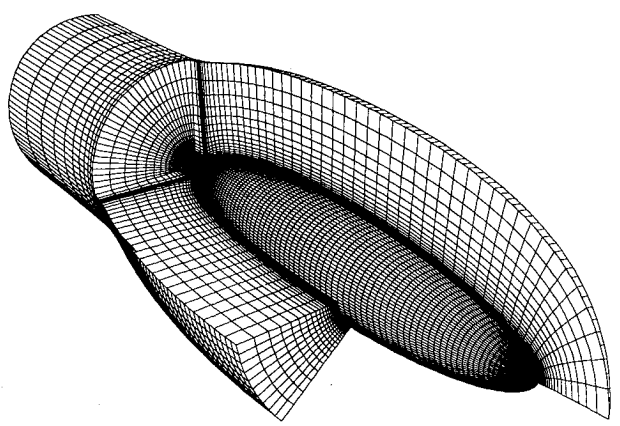

Fig. 1 Computational grid: for clarity, only part of the grid is shown.

Table 1 Turbulence models investigated

Model	Basic model	Modifications
A	Baldwin-Lomax	None
B	Baldwin-Lomax	Degani-Schiff
C	Johnson-King	Abid et al.,[5] three-dimensional ODE
D	Johnson-King (model C)	Degani-Schiff
E	Baldwin-Lomax	Panaras and Steger[6]

Baldwin-Lomax Turbulence Model Modifications

The Baldwin-Lomax model (model A) is used extensively because of its efficiency (leading to low computational time requirements) and its accuracy, which was found to be comparable to more complex turbulence models.[15] The Baldwin-Lomax model is patterned after an algebraic model developed by Cebeci et al.,[16] but uses modifications that simplify the determination of the edge of the boundary layer. In dimensional variables for turbulent flow computations, the viscosity μ and coefficient of thermal conductivity κ are assumed to be the sum of the laminar-flow coefficients and a turbulent-flow coefficient, i.e.,

$$\mu = \mu_l + \mu_t \tag{2}$$

$$\frac{\kappa}{c_p} = \frac{\mu_l}{Pr} + \frac{\mu_t}{Pr_t} \tag{3}$$

In Eq. (3), c_p denotes the specific heat at constant temperature. The turbulent flow is divided into an inner and outer region, and a different set of equations is used in each region to determine the turbulent eddy viscosity μ_t. The final value of μ_t is defined as

$$\mu_t = \min\left[(\mu_t)_{\text{inner}}, (\mu_t)_{\text{outer}}\right] \tag{4}$$

In the inner region, the Prandtl-Van Driest formulation is used to determine μ_t. This formula is defined as

$$\mu_{t,i} = \rho\, l^2\, \Omega \tag{5}$$

where

$$l = ky\left[1.0 - e^{-(y^+/A^+)}\right] \tag{6}$$

$$y^+ = \frac{\rho_w u_\tau y}{\mu_w} = \frac{\sqrt{\rho_w \tau_w}\, y}{\mu_w} \tag{7}$$

In Eq. (5), Ω is the magnitude of the local vorticity vector, which is defined in Cartesian space as

$$\Omega = \sqrt{(u_y - v_x)^2 + (v_z - w_y)^2 + (w_x - u_z)^2} \tag{8}$$

In the outer region, for attached boundary layers, μ_t is determined by use of the following equation:

$$\mu_{t,o} = KC_{cp}\rho F_{\text{wake}} F_{\text{Kleb}}(y) \tag{9}$$

In Eq. (9),

$$F_{\text{wake}} = \min\left[(y_{\max} F_{\max}), (C_{wk}\, y_{\max}\, u_{\text{dif}}^2)\right] \tag{10}$$

where u_{dif} is the difference between the maximum and minimum total velocity in the local profile[2]

$$u_{\text{dif}} = (\sqrt{u^2 + v^2 + w^2})_{\max} - (\sqrt{u^2 + v^2 + w^2})_{\min} \tag{11}$$

and F_{Kleb} is the Klebanoff intermittency factor

$$F_{\text{Kleb}}(y) = \left[1.0 + 5.5\left(\frac{C_{\text{Kleb}} y}{y_{\max}}\right)^6\right]^{-1} \tag{12}$$

The quantity $F_{\max}$ is defined as the maximum that the following function

$$F(y) = y\Omega[1.0 - e^{-(y^+/A^+)}] \tag{13}$$

takes in the local profile, and $y_{\max}$ is the normal distance from the surface at which this maximum occurs. The constants that appear in the preceding equations are given in Ref. 2.

A problem with the Baldwin-Lomax model (model A) is encountered when it is applied to treat flow about slender bodies at incidence.[17] In this flow regime, regions of crossflow separation dominate. In these separated flow regions, it becomes difficult to determine the correct values for $F_{\max}$, which, in turn, produces erroneous results for $\mu_{t,\text{outer}}$. This problem may be identified by analyzing the typical behavior of the function $F(y)$ in a region of attached flow and a region of crossflow separation (Figs. 2). In a region of attached flow, $F_{\max}$ is well defined, and it follows that the value of $y_{\max}$ is also well defined. However, in a region where a vortex structure resulting from crossflow separation exists, the function $F(y)$ is not well behaved. Here, two relative maxima are encountered. The first peak occurs within the boundary layer, and a second, larger peak exists due to the presence of the vortex sheet. If the Baldwin-Lomax model is used to search the entire flowfield normal to a surface point for $F_{\max}$, the second maximum in $F(y)$ is obtained, rather than the desired peak based on the underlying boundary layer. This results in values of $F_{\max}$ and $y_{\max}$ (and a value of $\mu_{t,\text{outer}}$) that are much too high, resulting in a distortion or a washout of the features in the computed flow. Specifically, the primary vortices would be smaller than those observed experimentally, and secondary separation and resulting secondary vortices generally are not determined.

To address this problem, Degani and Schiff[4] proposed a modification (model B) to the application of the model. Instead of searching outward along the entire radial ray for the value of $F_{\max}$ at each surface grid point, a criterion is established to differentiate between the two local maxima and to limit the search outward along the ray. A peak is found once the value of $F(y)$ drops to 90% of the local maximum value. The limit of the search is based on the $y_{\max}$ value of either the previous windward ray or the ray along the windward plane of symmetry. Along rays near the crossflow separation line, the two peaks tend to merge since the overlying vortex structure is close to the boundary layer, and no definite peak may occur. In this case, the eddy-viscosity coefficient is taken to be that found on the adjoining, more windward, ray. In this way, the Degani-Schiff modifications may be applied to a variety of local flow conditions and local Reynolds numbers. A recent discussion of the application of the Degani-Schiff modifications to compute high-incidence flow about ogive-cylinder bodies can be found in Ref. 18.

The flowfield investigated in this study was previously computed by Panaras and Steger,[6] who used the identical grid and flow solver. In this work, Panaras and Steger employed the Baldwin-Lomax model (model A) and their own modification to the Baldwin-Lomax model (model E). From the solution obtained using model A, they note that the first peak in $F(y)$ generally occurs close to the body surface. After reviewing the behavior of $F(y)$, they concluded that it is sufficient, in this case, to stop the outward search along each ray at some arbitrary l index, where l denotes the grid index normal to the body surface. For their computation of this flow, the search was stopped at $l = 22$. The solution obtained by Panaras and Steger using this cutoff index (model E) is included in this paper for comparison.

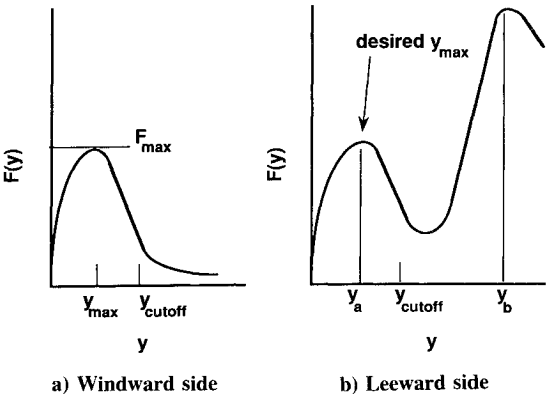

Fig. 2 Behavior of $F(y)$ at large incidence.[4]

Johnson-King Turbulence Model Modifications

Another turbulence model used in this study is one based on the model developed by Johnson and King.[3] The developers characterize this turbulence model as a half-equation, Reynolds stress, eddy-viscosity model, in which an ordinary differential equation (ODE) is used to determine the maximum Reynolds shear stress, rather than the partial differential equation (PDE) used in one-equation models. The closure model is composed of a nonequilibrium eddy-viscosity distribution, a rate equation for the streamwise development of the Reynolds shear stress $-\overline{u'v'}$, and an equilibrium eddy-viscosity distribution, in which production equals dissipation.[3] Originally developed for two-dimensional turbulent boundary layers, this model was extended to three dimensions by Abid et al.[5] and further modified in this work to utilize an ODE (for steady-state computations) in three-dimensional flows.

As with the Baldwin-Lomax model, the Johnson-King model divides the boundary layer into an inner and outer region. The turbulent eddy viscosity μ_t is a function of the viscosity values for these two regions and is assumed to be[19]

$$\mu_t = \mu_{t,o} \tanh\left(\mu_{t,i}/\mu_{t,o}\right) \tag{14}$$

where $\mu_{t,i}$ and $\mu_{t,o}$ describe the eddy viscosity in the inner and outer regions of the boundary layer, respectively. Equation (14) provides a smooth blending between the inner and outer regions of the boundary layer and makes μ_t dependent on $\mu_{t,o}$ across most of the boundary layer.

For attached, adverse pressure gradient conditions, the law-of-the-wall relationship near the surface is satisfied by defining the following relationship[19] for the inner eddy viscosity:

$$\mu_{t,i} = (1.0 - \gamma_2)(\mu_{t,i})_{M-L} + \gamma_2(\mu_{t,i})_{J-K} \tag{15}$$

where $(\mu_{t,i})_{M-L}$ is found using the Prandtl-Van Driest mixing-length formulation used in the Baldwin-Lomax model, and

$$(\mu_{t,i})_{J-K} = \rho D^2 \kappa y \sqrt{\rho_m/\rho}\, u_m \tag{16}$$

where u_m is the velocity scale and the subscript m denotes values evaluated at the location of maximum shear stress. In

Eq. (16), the damping term D is defined as[20]

$$D = 1.0 - \exp\left(\frac{-\rho_w y\sqrt{(\tau_w/\rho_w)}}{\mu_w A^+_{J-K}}\right) \tag{17}$$

with $A^+_{J-K} = 17$. The function γ_2 in Eq. (15) is defined[19] as

$$\gamma_2 = \tanh(y/L_c) \tag{18}$$

where

$$L_c = \frac{\sqrt{\rho_w}u_\tau L_m}{\sqrt{\rho_w}u_\tau + \sqrt{\rho_m}u_m} \tag{19}$$

The outer eddy viscosity term, as first proposed by Johnson and King,[3] is defined as

$$\mu_{t,o} = \sigma(x)Ku_e\delta^*_i F_{\text{Kleb}} \tag{20}$$

where F_{Kleb} is the Klebanoff intermittency function. Following Ref. 5, the Baldwin-Lomax formulation for the outer viscosity term is used in this model in order to simplify finding the edge of the boundary layer:

$$\mu_{t,o} = \sigma(x)KC_{cp}\rho F_{\text{wake}}F_{\text{Kleb}}(y) \tag{21}$$

For three-dimensional applications, the total Reynolds shear stress is defined as[21]

$$\tau = \mu_t\Omega/\rho \tag{22}$$

where Ω is the magnitude of the vorticity.

The unknown $\sigma(x)$ in the outer viscosity formulation provides the link between the assumed algebraic eddy-viscosity distribution and the rate equation for the streamwise development of the maximum Reynolds shear stress.[22] This rate equation is derived from the turbulent kinetic-energy equation. For three-dimensional flow, in Cartesian coordinates, this equation is defined as[21]

$$\frac{\partial\tau_m}{\partial t} + U_m\frac{\partial\tau_m}{\partial x} + V_m\frac{\partial\tau_m}{\partial y} + W_m\frac{\partial\tau_m}{\partial z} = \frac{\alpha_1}{L_m}[(\tau_{m,\text{eq}})^{1/2} - (\tau_m)^{1/2}] - a_1D_m \tag{23}$$

where

$$L_m = \min(0.4N_m, 0.09\delta) \tag{24}$$

and

$$D_m = \frac{C_D\tau_m^{3/2}|1.0 - \sigma^{1/2}|}{a_1[0.7\delta - N_m]} \tag{25}$$

where L_m is the dissipation length scale, D_m the turbulent diffusion term, τ_m the maximum shear stress value in the local profile, N_m the normal distance from the surface at which the maximum shear stress occurs, and δ the boundary-layer thickness. The constants C_D and a_1 are defined in Ref. 3.

A streamline method[23] is used to solve Eq. (23). If a streamline coordinate system (s,n) is chosen, the rate equation, Eq. (23), is rewritten as follows:

$$\frac{\partial\tau_m}{\partial t} + U_s\frac{\partial\tau_m}{\partial s} = \frac{a_1}{L_m}\tau_m[(\tau_{m,\text{eq}})^{1/2} - (\tau_m)^{1/2}] - a_1D_m \tag{26}$$

Making the following change in variables

$$g = \tau_m^{-1/2} \tag{27a}$$

$$g_{\text{eq}} = \tau_{m,\text{eq}}^{-1/2} \tag{27b}$$

Eq. (26) is rewritten as follows:

$$\frac{\partial g}{\partial t} + U_s\frac{\partial g}{\partial s} = -\frac{a_1}{2L_m}\left[\left(\frac{g}{g_{\text{eq}}} - 1.0\right) - \frac{C_D L_m|1.0 - \sigma^{1/2}|}{a_1(0.7\delta - N_m)}\right] \tag{28}$$

The steady-state form of Eq. (28) is an ODE and is solved using Euler's method. Knowing the velocity components of the flow at the location of τ_m along the ray normal to a given surface grid point, it is possible to calculate the direction of the flow and, thus, the direction of the shear stress equation and to determine where the streamline crosses the upstream axial station. The values of the terms on the right side of Eq. (28) are found by linear interpolation of the values at the grid points neighboring the streamline at the upstream axial station.

To link the maximum shear stress value as determined from the rate equation and the maximum shear stress value as determined from the eddy viscosity distribution of the flowfield, the term $\sigma(x)$ is used. The value of $\sigma(x)$ is found using the following equation:

$$\sigma^{t+\text{dt}} = \sigma^t\frac{\rho_{\max}\tau_m}{(\mu_t\Omega)_{\max}} \tag{29}$$

where τ_m is determined from the ODE and $(\mu_t\Omega)_{\max}$ from the shear stress distribution of the previous time step. An iteration procedure is used within each time step to refine the value of $\sigma(x)$ such that the maximum shear stress from the profile equals the value obtained from the ODE.

This model is used after a converged solution is obtained using an equilibrium eddy-viscosity turbulence model, such as the Baldwin-Lomax model. The initial conditions for the ODE are taken to be as follows:

$$\mu_t = \mu_{t,\text{eq}} \tag{30a}$$

$$g = g_{\text{eq}} \tag{30b}$$

The solution is then reconverged using this model. Using the eddy viscosity values of the previous time step, the shear stress distribution in the flowfield is determined from Eq. (22). At each surface grid point in a given axial plane, the ray normal to the body is searched to find τ_m. Equation (28) is then solved using the data from the previous time step to determine the right-hand side. Knowing τ_m from the ODE, new values of $\sigma(x)$ are determined from which the new turbulent eddy-viscosity values are computed.

Following Ref. 19, D_m was set to zero in regions of attached flow. In addition, per Ref. 5, the boundary-layer thickness δ is taken to be 1.9 $y_{\max}$, where $y_{\max}$ is the same $y_{\max}$ used in the Baldwin-Lomax model.[2] Finally, the equilibrium shear stress value $\tau_{m,\text{eq}}$ in Eq. (23) is determined using the following formula for the inner viscosity value:

$$(\mu_{t,i})_{\text{eq}} = \rho D^2\kappa y\sqrt{\rho_m/\rho}u_{m,\text{eq}} \tag{31}$$

and setting $\sigma(x) = 1.0$ in the equation for the outer viscosity value, Eq. (21). The equilibrium turbulent eddy-viscosity coefficient is then determined using Eq. (14).

In this study, model C is the Johnson-King model using the Baldwin-Lomax equations to determine the outer eddy viscosity, following the modifications of Abid et al.[5] Since the prolate spheroid is a body of revolution at high angle of attack, where crossflow separation is an important factor, the Degani-Schiff modifications to the Baldwin-Lomax model are incorporated into model C to form model D.

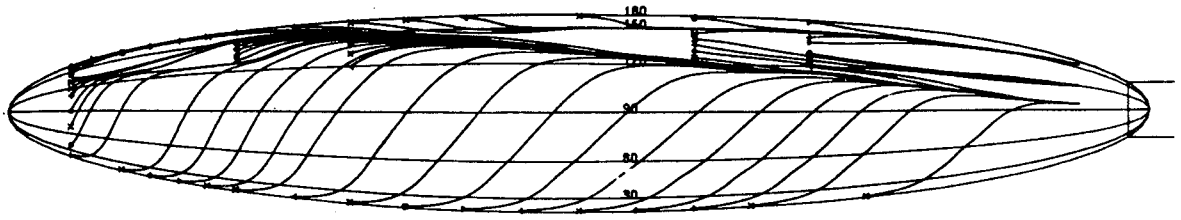

Fig. 3 Surface limiting streamline pattern: $M_\infty = 0.13$; $\alpha = 27$ deg; $Re_D = 1.1 \times 10^6$ (Ref. 27).

Results and Discussion

The accuracy of a computational solution depends on the flow solver, the grid resolution, and the turbulence model used. Previous work[1] focused on the effects of different flow solvers and degrees of grid resolution on the flowfield about a prolate spheroid at high angle of attack. The present study investigates the effect of the turbulence model on such a solution. The case for which solutions are computed corresponds to experiments performed at the ONERA wind-tunnel facility by Meier,[24] Meier and Kreplin,[25,26] and Kreplin et al.[27] on a 6:1 prolate spheroid. This configuration was tested extensively at the DFVLR to study three-dimensional separated flow. The flow conditions for the case in question are $M_\infty = 0.25$, $\alpha = 30$ deg, and Reynolds number (based on maximum body diameter and freestream conditions) of $Re_D = 7.2 \times 10^6$. For this high Reynolds number flow, laminar and transitional effects should be limited to a small region at the nose of the body. Thus, in the computations, the flow is assumed to be fully turbulent, and the turbulence model is applied over the entire body. Solutions are obtained using the four turbulence models described in the previous section. These solutions are compared to experimental pressure data[24] and to previous computational results obtained by Panaras and Steger[6] using the same solver and identical grid and different turbulence model (model E). The solutions are analyzed using surface flow patterns, helicity density contours, pressure distributions, and turbulent eddy-viscosity profiles.

The computational grid consists of 121 axial, 53 circumferential, and 65 normal points (Fig. 1), defining the prolate spheroid, an attached sting, and the surrounding flowfield. The computational grid extends circumferentially halfway around the body, and an implicit plane-of-symmetry boundary condition is employed. A no-slip condition is used at the body surface and along the sting. The computational grid extends 11 body lengths ahead of the nose and 14 body lengths above and below the body. At the outer surface of the grid, undisturbed freestream conditions are maintained.

Surface Flow Patterns

The prolate spheroid body used in this study was tested extensively at the DFVLR[24-27] in investigations of three-dimensional separated flow. Surface pressure distributions were measured over a wide range of flow conditions,[24,26] including Reynolds numbers ranging up to $Re_D = 7.2 \times 10^6$. At this high Reynolds number, laminar and transitional crossflow separation effects are limited to a small region near the nose of the body. Therefore, this case was selected and the flow is assumed to be fully turbulent in the computations. In addition, surface oil flow patterns[26] and wall shear stress data[27] were obtained, albeit at a lower Reynolds number, $Re_D = 1.1 \times 10^6$. At this lower Reynolds number, the region of laminar and transitional crossflow separation is more extensive. However, excluding the region close to the nose, the main features of the surface flow pattern are common to both Reynolds number cases and may be observed in Fig. 3. In this figure, the limiting streamlines are obtained from the wall shear stress data and plotted to illustrate the flow pattern on the surface of the body. Typically, for a prolate spheroid, there is a primary crossflow separation line, beginning near the nose, and a secondary crossflow separation line, beginning near the half-body station. These lines are formed by the convergence of the surface streamlines, or skin-friction lines.[28] The separation lines indicate the locations where the boundary layer separates from the body surface to form vortex sheets, which then feed the primary and secondary vortices above the leeward side of the body.

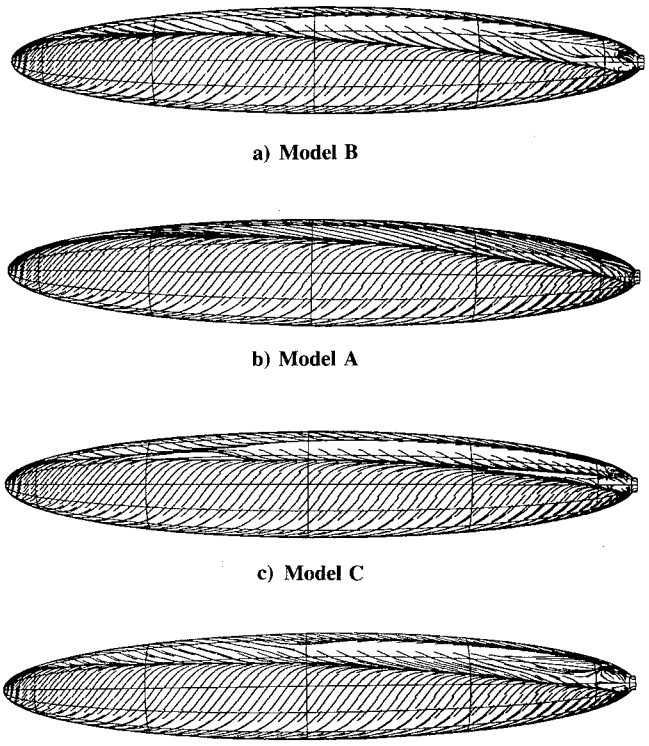

a) Model B

b) Model A

c) Model C

d) Model D

Fig. 4 Surface flow patterns: $M_\infty = 0.25$; $\alpha = 30$ deg; $Re_D = 7.2 \times 10^6$.

The computed solution obtained using model B yields a fairly accurate solution, in terms of the surface flow pattern (Fig. 4a). In this case, both the primary and secondary lines are well defined, along with a tertiary line near the rear of the body. Schiff and Sturek[17] and Panaras and Steger[6] found that a solution obtained using model A did not capture the secondary separation line for a body of revolution at incidence. The same result is observed in the present solution obtained using model A (Fig. 4b). The primary crossflow separation line occurs leeward of the line obtained using model B. This finding is in agreement with results obtained using these two models in a previous study of flow over tangent-ogive cylinders.[10] The solution using model C is also capable of capturing the primary and secondary crossflow separation lines (Fig. 4c) as well as the beginnings of a tertiary separation line. However, in Fig. 4c, the primary and secondary lines seem to merge near the nose, which is physically incorrect. This is apparently due to the use of the unmodified Baldwin-Lomax outer layer eddy-viscosity equation. The solution obtained using model D yields a surface flow pattern (Fig. 4d) closely resembling the solution using model B. Therefore, for this case, where crossflow separation is a consideration, the use

of the unmodified Baldwin-Lomax outer layer eddy-viscosity equation has an adverse effect on the accuracy of the Johnson-King model.

Off-Surface Flow Structures

Surface flow patterns provide a means of visualizing the flow near the surface of the body. To visualize the flow off the body and to examine the vortex structure on the leeward side of the body, helicity density contours are employed. Helicity density is defined[29] as the scalar product of the velocity and vorticity vectors. Therefore, these contours can show both the relative magnitude and direction of rotation of the vortices. A comparison of the helicity density contours shows how the turbulence models can affect the off-surface flow structures.

The solution obtained using model B indicates both the primary and secondary vortices (Fig. 5a). Note that the secondary vortices, located under the primary vortices, rotate in a direction opposite to that of the primary ones. The helicity density plot of the solution using model A shows only the primary vortex (Fig. 5b), corresponding to the primary separation line in the surface flow pattern. Furthermore, note that the primary vortex is fairly small compared to the other solutions. The solution using model C produces vortices that

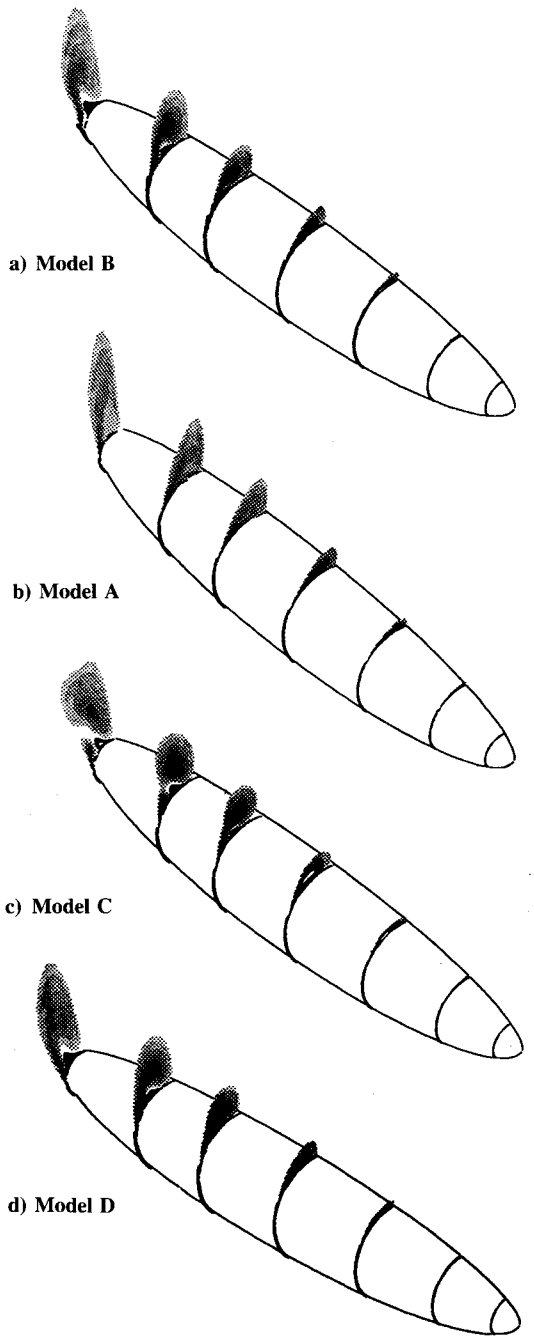

Fig. 5 Computed off-surface vortical flow structures, visualized using helicity density contours: $M_\infty = 0.25$; $\alpha = 30$ deg; $Re_D = 7.2 \times 10^6$.

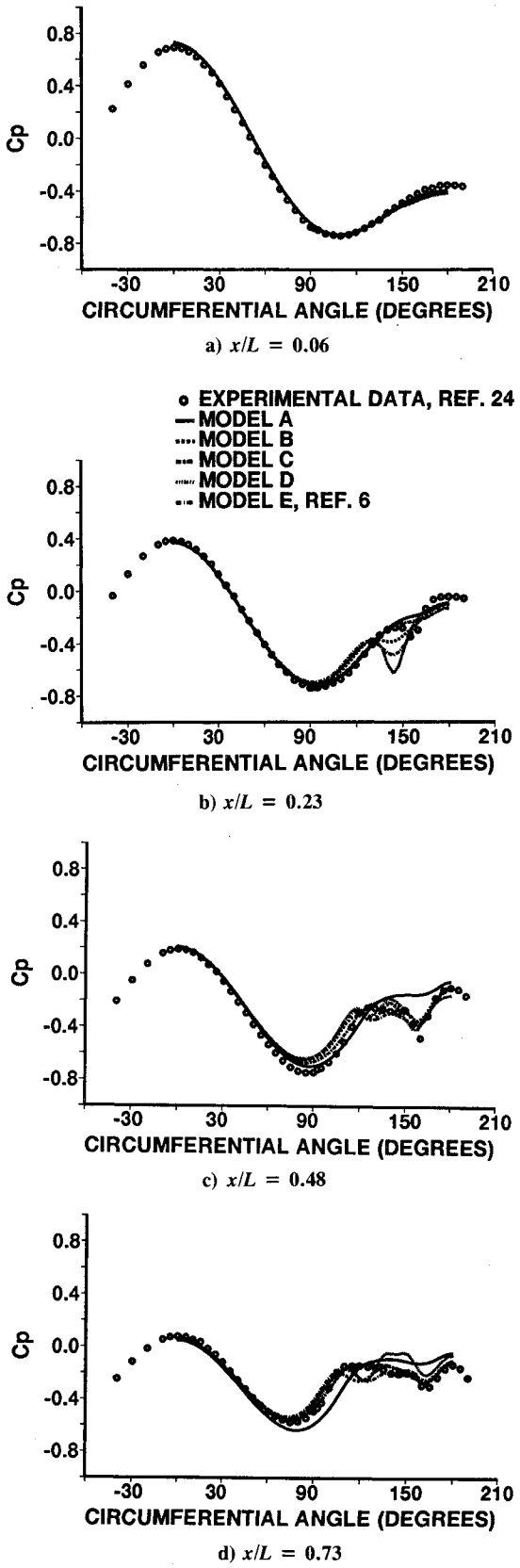

Fig. 6 Surface pressure distributions: $M_\infty = 0.25$; $\alpha = 30$ deg; $Re_D = 7.2 \times 10^6$.

are of the same magnitude as the solution using model B, but the shape of the vortices is different, especially near the rear of the body (Fig. 5c). However, as was the case with the surface flow pattern, the model D solution (Fig. 5d) yields results similar to those obtained using model B.

Surface Pressure

Both the surface flow patterns and the helicity density contours provide a qualitative measure of solution accuracy. To obtain a quantitative measure of accuracy, comparison to some experimentally determined flow variable must be made. For the case studied, experimental surface pressure results are available.[24] Figure 6 compares computed and experimental values. Computed results are determined for the half-body between $\phi = 0$ deg (windward) and $\phi = 180$ deg (leeward), whereas experimental values are available from -40 deg $< \phi < 190$ deg. Although vortex symmetry can occur for bodies of revolution at high incidence (cf. Ref. 30), such asymmetry is not expected for the blunt-nosed body and flow conditions investigated in this study. Experimental pressure data (Figs. 6) indicate that, in this case, the flow is symmetrical. Therefore, the use of a grid with an implicit plane-of-symmetry condition is justified.

Surface pressure coefficients are compared at four axial stations. The first station is the closest experimental station to the nose of the body, at $x/L = 0.0555$ (Fig. 6a). In this region, the flow is still attached and all of the computed values compare well with experiment. This is expected since the Baldwin-Lomax model and the Johnson-King model work well for attached flows in a favorable pressure gradient. Moving aft along the body (Figs. 6b–d), certain trends appear. In the attached, windward region, computational values agree well with experimental values. In the leeward region, the solutions using models A and E exhibit a pressure rise leeward of the other computed solutions. The solution using model A predicts higher-than-experimental pressures in the region from 120 deg $< \phi$ 180 deg, especially at the axial locations where the secondary crossflow separation lines appear. The solution using model C predicts a larger pressure drop at the one-quarter body station, and a larger pressure rise at the three-quarter body station, compared to the experimental values. However, as with the solutions using models B and D, the

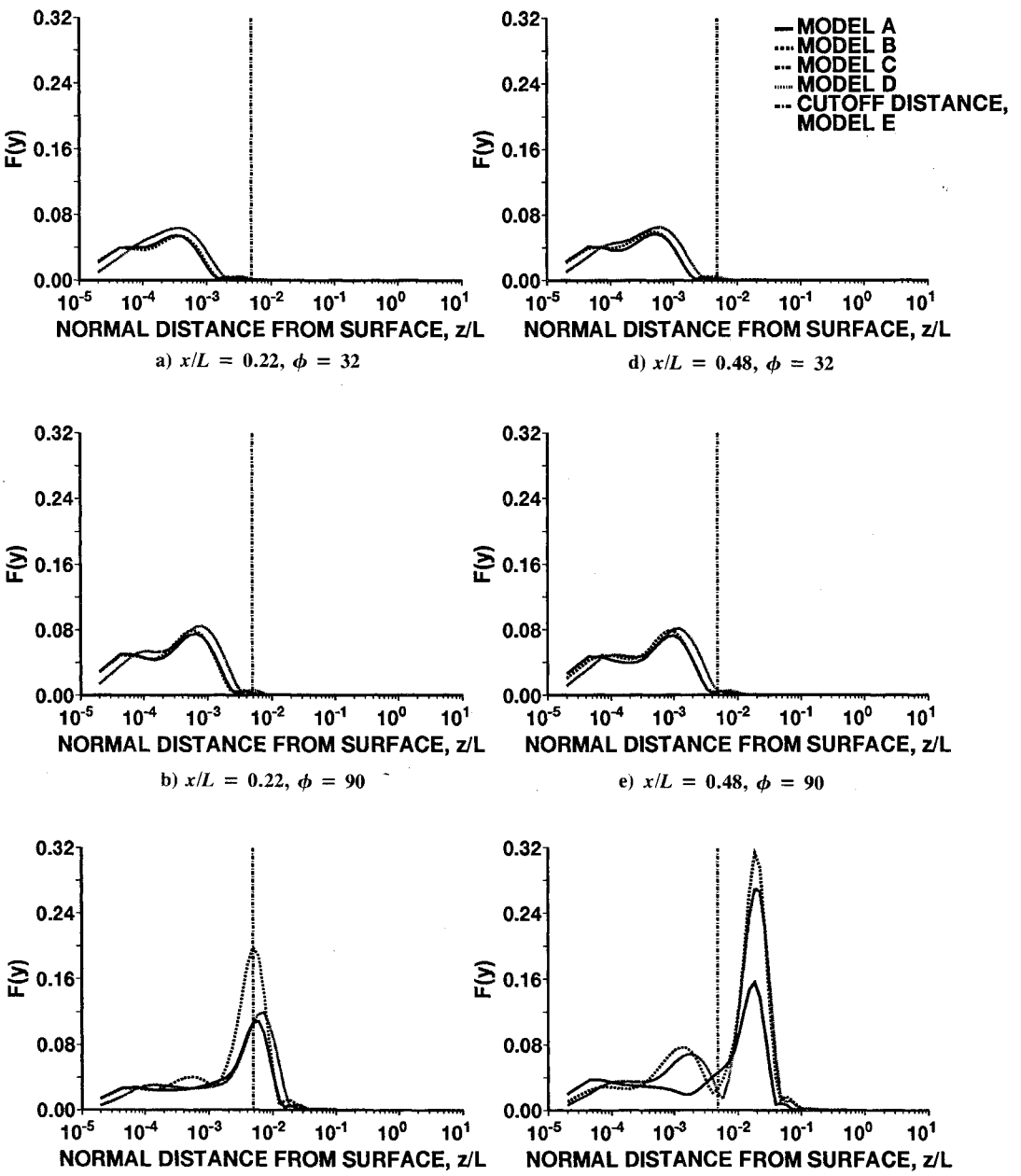

a) $x/L = 0.22$, $\phi = 32$

d) $x/L = 0.48$, $\phi = 32$

b) $x/L = 0.22$, $\phi = 90$

e) $x/L = 0.48$, $\phi = 90$

c) $x/L = 0.22$, $\phi = 151$

f) $x/L = 0.48$, $\phi = 151$

Fig. 7 Profiles of $F(y)$ at various axial and circumferential locations: $M_\infty = 0.25$; $\alpha = 30$ deg; $Re_D = 7.2 \times 10^6$.

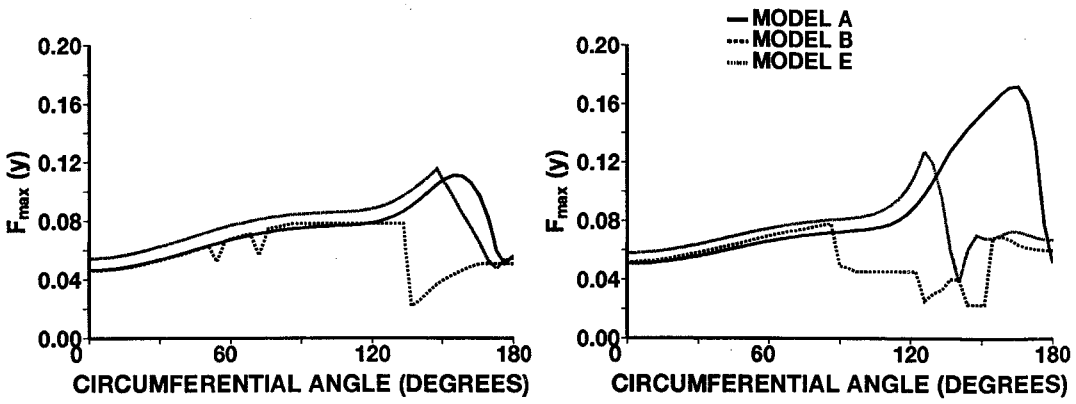

a) $x/L = 0.23$ b) $x/L = 0.48$

Fig. 8 Circumferential distribution of F_{max} at various axial stations: $M_\infty = 0.25$; $\alpha = 30$ deg; $Re_D = 7.2 \times 10^6$.

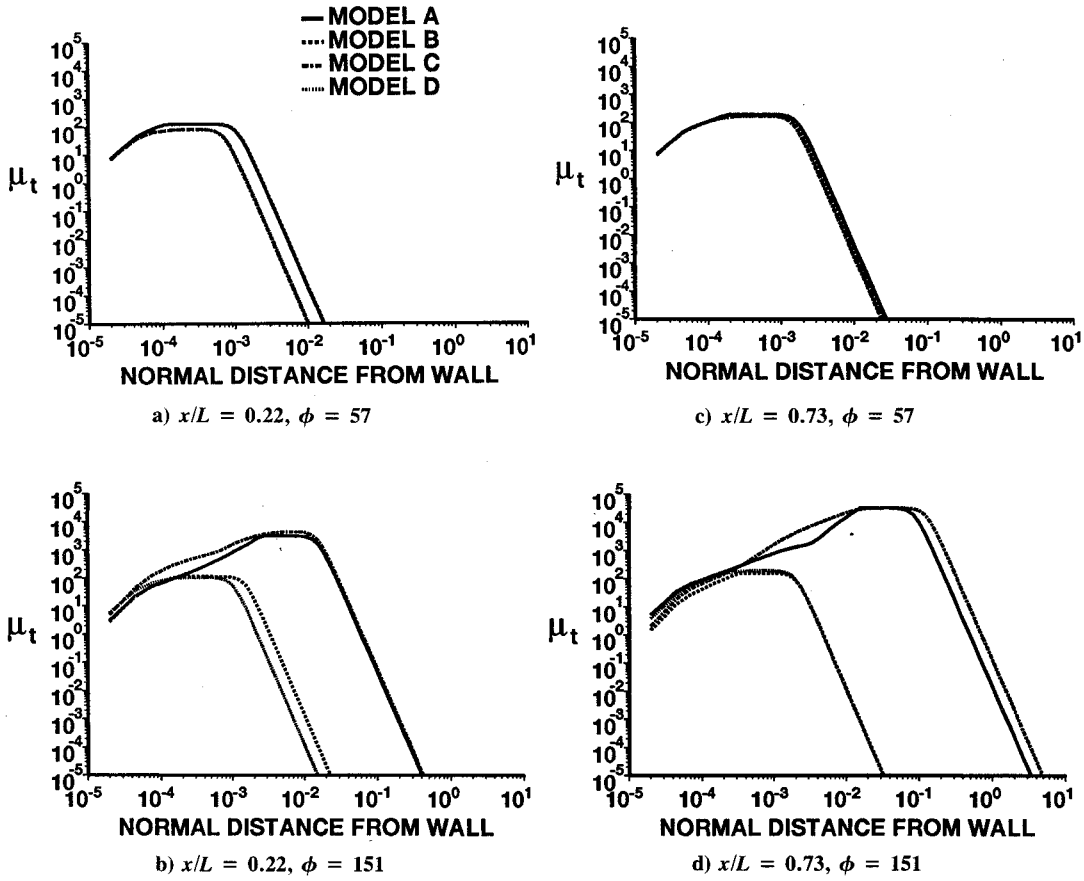

a) $x/L = 0.22$, $\phi = 57$ c) $x/L = 0.73$, $\phi = 57$

b) $x/L = 0.22$, $\phi = 151$ d) $x/L = 0.73$, $\phi = 151$

Fig. 9 Profiles of μ_t at two leeward and windward stations: $M_\infty = 0.25$; $\alpha = 30$ deg; $Re_D = 7.2 \times 10^6$.

solution using model C captures the qualitative features of the circumferential pressure distribution, i.e., the adverse circumferential pressure gradients corresponding to the primary and secondary crossflow separation lines. Quantitatively, though, the solutions using models B and D provide the better results of the four solutions computed in this study.

Turbulent Eddy-Viscosity Distributions

It was determined that model A (the unmodified Baldwin-Lomax model) did not capture the flow characteristics accurately in flows where crossflow separation is important. Attempts to modify the model to compensate for this shortcoming were made by Degani and Schiff[4] and Panaras and Steger.[6] As stated previously, the Baldwin-Lomax model depends on a function $F(y)$ of the vorticity magnitude Ω to determine the outer layer eddy viscosity. Studying the behavior of this function at various points on the body, and comparing the values of F_{max} and y_{max} obtained using the various modifications to the Baldwin-Lomax model, gives an indication of the effects of these modifications on the Baldwin-Lomax model.

Figures 7 show a comparison of profiles of $F(y)$ at a number of circumferential locations along two axial stations. Profiles at $x/L = 0.22$ and several circumferential locations are shown in Figs. 7a–c. The cutoff distance marker in Figs. 7 corresponds to the $l = 22$ plane used by Panaras and Steger[6] to limit their search for F_{max}. In the separated region, $\phi = 151.2$ deg (Fig. 7c), the maximum corresponding to the vortex sheet occurs within the cutoff region, meaning that the Panaras and Steger modification (model E) does not choose the first local maximum. Figure 8a indicates that both models A and E use the maximum shown in Fig. 7c to compute the turbulent eddy-

viscosity coefficient. The Degani-Schiff modifications (model B) yield two results. First, in the region 90 deg $< \phi <$ 120 deg, a local maximum could not be determined within the cutoff distance set for this axial station (Fig. 7b); thus, the value from the previous windward ray is used (Fig. 8a). This region corresponds to the general location of the primary crossflow separation line. Between 120 deg $< \phi <$ 180 deg, the vortex sheet is sufficiently separated from the body (Fig. 7c), such that the 90% selection criterion employed by Degani and Schiff is again applicable, and the first local maximum is selected (Fig. 8a). This corresponds to an order of magnitude difference in the value of y_{max} between model B and models A and E. At the $x/L = 0.48$ axial station (Figs. 7d–f), the primary vortex lifts far enough from the body that the search cutoff criterion employed by Panaras and Steger[6] works correctly, causing the model to select the first local maximum (Fig. 8b). At this station, this corresponds to the value of F_{max} and y_{max} chosen by model B. This explains why the model E solution resolves the secondary separation line, whereas the model A solution does not. Note that, at both axial stations, the values of F_{max} in the attached, windward region (Figs. 8) are approximately the same for each of the solutions shown.

Since all of the models investigated use the Baldwin-Lomax outer layer formula, the $F(y)$ distribution and the values of F_{max} and y_{max} selected have a bearing on the turbulent eddy-viscosity values obtained from each of the models. The eddy-viscosity profiles at two windward and leeward stations are shown in Figs. 9. In the attached, windward region (Figs. 9a and 9c), the turbulent eddy-viscosity profiles are approximately the same, in agreement with the idea that all of the models investigated give similar results for attached flows in a favorable pressure gradient. In the separated flow region (Figs. 9b and 9d), the viscosity coefficients fall into two groupings. Models A and C yield values much greater than models B and D, indicating the effect of the Degani-Schiff modifications. This is due to the differences in F_{max} and y_{max} observed earlier. A large value of y_{max} will increase F_{wake} in Eq. (10) and decrease $F_{Kleb}(y)$ in Eq. (12). This results in large values of $\mu_{t,o}$ as well as a delay in the effect of the Klebanoff intermittency factor, leading to the large difference between the two groupings shown in Figs. 9b and 9d. Since the groupings in Figs. 9b and 9d depend on the use of Degani-Schiff modifications, it appears that, for the body and flow investigated in this study, the form of the Johnson-King model used in this study cannot correct the discrepancies introduced by the Baldwin-Lomax outer layer formulation. Furthermore, the small differences in the eddy-viscosity values between models A and C and between models B and D indicate that the nonequilibrium effects are small. That is, for this slender body flow, the maximum Reynolds shear stress does not undergo rapid changes in the streamwise direction.

Conclusions

Three-dimensional separated flow about a prolate spheroid is computed numerically using a thin-layer Navier-Stokes code, F3D, and four turbulence models. The turbulence models are the Baldwin-Lomax model (model A), the Baldwin-Lomax model as modified to account for crossflow separation by Degani and Schiff (model B), a modified form of the Johnson-King model extended to three dimensions using an ODE for the rate equation and incorporating the Baldwin-Lomax outer layer eddy-viscosity formula (model C), and with the Degani-Schiff modifications (model D). Steady, fully turbulent flow about a prolate spheroid at $M_\infty = 0.25$, $\alpha = 30$ deg, and $Re_D = 7.2 \times 10^6$ is computed. The computed solutions are compared with experimental pressure data and analyzed using surface flow patterns, helicity density contours, and turbulent eddy-viscosity profiles.

The solution using the Baldwin-Lomax model (model A) does not capture the secondary separation line near the surface and generally predicts higher pressures in the leeward region than those measured experimentally. The eddy-viscosity values obtained from the model are quite large compared to the other models, leading to a less-energetic flow characterized by a weak primary vortex. This is in keeping with previous results obtained for bodies of revolution at high incidence using this turbulence model. With the Degani-Schiff modified Baldwin-Lomax model (model B), a solution is obtained that captures both the primary and secondary separation lines, as well as a tertiary line near the base of the body. The surface pressures match quite well with experiment, although the pressure rises and drops associated with flow separation occur slightly windward from those obtained from the experiment. Furthermore, the modifications developed by Degani and Schiff[4] to account for the crossflow separation are more effective in selecting the first local maximum in the $F(y)$ profile than the simpler criterion used by Panaras and Steger.[6]

The solution using model C resolves the primary and secondary separation lines, although these two lines seem to merge together near the nose of the body. After the Degani-Schiff modifications are applied to model C (model D), this discrepancy in the surface flow pattern disappears. Examination of the behavior of the $F(y)$ function used in the Baldwin-Lomax outer layer formulation, and comparison of the turbulent eddy-viscosity values obtained by the various models, leads to the conclusion that the discrepancy in the model C solution is due to the use of the Baldwin-Lomax outer layer eddy-viscosity formulation in the Johnson-King model. The similarity between the predicted flowfields and eddy-viscosity profiles obtained from solutions using models B and D implies that the nonequilibrium effects in this slender body flow are less than those for transonic wing flows.[5,21] However, for the body and flow conditions used in this study, more experimental data may be required before a better understanding of the effects of turbulence models on flow parameters can be gained.

Acknowledgments

This work was funded by NASA Grant NCC 2-564. The authors wish to thank Dennis A. Johnson for the helpful discussions concerning the application of the Johnson-King turbulence model and Joseph L. Steger for making his prolate spheroid results available.

References

[1]Vatsa, V. N., Thomas, J. L., and Wedan, B. W., "Navier-Stokes Computations of Prolate Spheroids at Angle of Attack," *AIAA Journal*, Vol. 26, No. 11, 1989, pp. 986–993.

[2]Baldwin, B., and Lomax, H., "Thin-Layer Approximation and Algebraic Model for Separated Turbulent Flows," AIAA Paper 78-0257, Jan. 1978.

[3]Johnson, D. A., and King, L. S., "A New Turbulence Closure Model for Boundary Layer Flows with Strong Adverse Pressure Gradients and Separation," AIAA Paper 84-0175, Jan. 1984.

[4]Degani, D., and Schiff, L. B., "Computation of Turbulent Supersonic Flows Around Pointed Bodies Having Crossflow Separation," *Journal of Computational Physics*, Vol. 66, No. 1, 1986, pp. 173–196.

[5]Abid, R., Vatsa, V. N., Johnson, D. A., and Wedan, B. W., "Prediction of Separated Transonic Wing Flows with a Non-Equilibrium Algebraic Model," AIAA Paper 89-0558, Jan. 1989.

[6]Panaras, A. G., and Steger, J. L., "A Thin-layer Solution of the Flow About a Prolate Spheroid," *Zeitschrift für Flugwissenschaften und Weltraumforschung*, Vol. 12, No. 3, 1988, pp. 173–180.

[7]Steger, J. L., "Implicit Finite-Difference Simulation of Flow About Arbitrary Two-Dimensional Geometries," *AIAA Journal*, Vol. 16, No. 7, 1978, pp. 679–686.

[8]Steger, J. L., Ying, S. X., and Schiff, L. B., "A Partially Flux-Split Algorithm for Numerical Simulation of Unsteady Viscous Flows," *Proceedings of a Workshop on Computational Fluid Dynamics*, Univ. of California, Davis, CA, 1986.

[9]Steger, J. L., and Warming, R. F., "Flux Vector Splitting of the Inviscid Gasdynamic Equations with Applications to Finite-Difference Methods," *Journal of Computational Physics*, Vol. 40, No. 2,

1981, pp. 263–293.

[10]Schiff, L. B., Degani, D., and Cummings, R. M., "Numerical Simulation of Separated and Vortical Flows on Bodies at Large Angles of Attack," *Fourth Symposium on Numerical and Physical Aspects of Aerodynamic Flows*, Long Beach, CA, Jan. 1989.

[11]Ying, S. X., Schiff, L. B., and Steger, J. L., "A Numerical Study of Three-Dimensional Separated Flow Past a Hemisphere Cylinder," AIAA Paper 87-1207, June 1987.

[12]Schiff, L. B., Cummings, R. M., Sorenson, R. L., and Rizk, Y. M., "Numerical Simulation of High-Incidence Flow over the F-18 Fuselage Forebody," AIAA paper 89-0339, Jan. 1989.

[13]Cummings, R. M., Rizk, Y. M., Schiff, L. B., and Chaderjian, N. M., "Navier-Stokes Predictions of the Flowfield Around the F-18 (HARV) Wing and Fuselage at Large Incidence," AIAA Paper 90-0099, Jan. 1990.

[14]Ying, S. X., "Three-Dimensional Implicit Approximately Factored Schemes for Equations in Gasdynamics," Ph.D. Dissertation, Stanford Univ, Stanford, CA, June 1986; also SUDAAR 557, June 1986.

[15]York, B., and Knight, D., "Calculation of a Class of Two-Dimensional Turbulent Boundary Layers Using the Baldwin-Lomax Model," AIAA Paper 85-0126, Jan. 1985.

[16]Cebeci, T., Smith, A. M. O., and Mosinkis, G., "Calculation of Compressible Adiabatic Turbulent Boundary Layers," *AIAA Journal*, Vol. 8, No. 11, 1970, pp. 1974–1982.

[17]Schiff, L. B., and Sturek, W. B., "Numerical Simulation of Steady Supersonic Flow Over an Ogive-Cylinder-Boattail Body," AIAA Paper 80-0066, Jan. 1980.

[18]Degani, D., Schiff, L. B., and Levy, Y., "Physical Considerations Governing Computation of Turbulent Flows Over Bodies at Large Incidence," AIAA Paper 90-0096, Jan. 1990.

[19]Johnson, D. A., and Coakley, T. J., "Improvements to a Nonequillibrium Algebraic Turbulence Model," *AIAA Journal*, Vol. 28, No. 11, 1990, pp. 2000–2003.

[20]Shirazi, S. A., and Truman, C. R., "A Study of Algebraic Half-Equation Turbulence Models for Hypersonic PNS Predictions," AIAA Paper 88-0222, Jan. 1988.

[21]Abid, R., and Johnson, D. A., "Effects of Turbulence Models on the Prediction of Transonic Wing Flows," Society of Automotive Engineers, Warrendale, PA, TP-892224, Sept. 1989.

[22]Johnson, D. A., "Predictions of Transonic Separated Flow with an Eddy-Viscosity/Reynolds Shear-Stress Closure Model," AIAA Paper 85-1683, July 1985.

[23]Johnson, D. A., private communication, Sept. 1989.

[24]Meier, H. U., private communication, Jan. 1989.

[25]Meier, H. U., and Kreplin, H.-P., "Experimental Investigation of the Boundary Layer Transition and Separation on a Body of Revolution," *Zeitschrift für Flugwissenschaften und Weltraumforschung*, Vol. 4, No. 2, 1980, p. 65–71.

[26]Meier, H. U., and Kreplin, H.-P., "Pressure Distributions and Flow Visualizations on a Ellipsoid 1:6 Designed for Three-Dimensional Boundary Layer Investigation," *Boundary Layer Effects — Proceedings of the 7th Air Force/Federal Republic of Germany Data Exchange Agreement Meeting*, Air Force Flight Dynamics Lab., AFFDL-TR-78-111, Wright-Patterson AFB, OH, 1978, pp. 197–208.

[27]Kreplin, H.-P., Vollmers, H., and Meier, H. U., "Experimental Determination of Wall Shear Stress Vectors on an Inclined Prolate Spheroid," *Viscous and Interacting Flow Field Effects — Proceedings of the 5th Air Force and the Federal Republic of Germany Data Exchange Agreement Meeting*, Air Force Flight Dynamics Lab., AFFDL-TR-80-3088, Wright-Patterson AFB, OH, 1980, pp. 315–332.

[28]Tobak, M., and Peake, D. J., "Topology of Three-Dimensional Separated Flows," *Annual Review of Fluid Mechanics*, Vol. 14, 1982, pp. 61–85.

[29]Levy, Y., Seginer, A., and Degani, D., "Graphical Representation of Three-Dimensional Vortical Flows by Means of Helicity Density and Normalized Helicity," AIAA Paper 88-2598, June 1988.

[30]Degani, D., and Zilliac, G. G., "Experimental Study of the Nonsteady Asymmetric Flow Around an Ogive-Cylinder at Incidence," *AIAA Journal*, Vol. 28, No. 4, 1990, pp. 642–649.